PAPER • OPEN ACCESS

UV-solvent annealing of PDMS-majority and PS-majority PS-*b*-PDMS block copolymer films

To cite this article: Keehong Lee *et al* 2016 *Nanotechnology* **27** 465301

View the article online for updates and enhancements.

Related content

- Morphology, directed self-assembly and pattern transfer from a high molecular weight polystyrene-block-poly(dimethylsiloxane) block copolymer film
Li-Chen Cheng, Wubin Bai, Eduardo Fernandez Martin et al.

- Universal pattern transfer methods for metal nanostructures by block copolymer lithography
Kun-Hua Tu, Wubin Bai, George Liontos et al.

- Nanoscale Silicon Substrate Patterns From Self-assembly of Cylinder Forming Poly(styrene)-block-poly(dimethylsiloxane) Block Copolymer on Silane Functionalized Surfaces
Dipu Borah, Cian Cummins, Sozaraj Rasappa et al.

This content was downloaded from IP address 18.101.8.74 on 17/10/2017 at 00:13

OPEN ACCESS
IOP Publishing

Nanotechnology

Nanotechnology **27** (2016) 465301 (11pp)

doi:10.1088/0957-4484/27/46/465301

UV-solvent annealing of PDMS-majority and PS-majority PS-*b*-PDMS block copolymer films

Keehong Lee[1,2,5], Melissa Kreider[1,5], Wubin Bai[1], Li-Chen Cheng[1], Saman Safari Dinachali[1], Kun-Hua Tu[1], Tao Huang[1,4], K Ntetsikas[3], G Liontos[3], A Avgeropoulos[3] and C A Ross[1]

[1] Department of Materials Science and Engineering, MIT, Cambridge MA 02139, USA
[2] Semiconductor R&D Center, Samsung Electronics, Hwasung-City, Gyeonggi-do, Korea
[3] Department of Materials Science Engineering, University of Ioannina, University Campus-Dourouti, 45110 Ioannina, Greece
[4] Department of Organic and Polymeric Materials, Tokyo Institute of Technology, Japan

E-mail: caross@mit.edu

Received 5 July 2016, revised 6 September 2016
Accepted for publication 12 September 2016
Published 13 October 2016

Abstract

The response of polystyrene-block-poly(dimethylsiloxane) (PS-*b*-PDMS) thin films to UV exposure during solvent vapor annealing is described, in order to improve their applicability in nanolithography and nanofabrication. Two BCPs were examined, one with the PS block as majority ($f_{PS} = 68\%$, $M_n = 53\ kg\ mol^{-1}$), the other with PDMS block as majority ($f_{PDMS} = 67\%$, $M_n = 44\ kg\ mol^{-1}$). A 5 min UV irradiation was applied during solvent vapor annealing which led to both partial crosslinking of the polymer and a small increase in the temperature of the annealing chamber. This approach was effective for improving the correlation length of the self-assembled microdomain arrays and in limiting subsequent flow of the PDMS in the PDMS-majority BCP to preserve the post-anneal morphology. Ordering and orientation of microdomains were controlled by directed self-assembly of the BCPs in trench substrates. Highly-ordered perpendicular nanochannel arrays were obtained in the PDMS-majority BCP.

S Online supplementary data available from stacks.iop.org/NANO/27/465301/mmedia

Keywords: block copolymer, solvent vapor annealing, UV irradiation, microphase separation, directed self-assembly, thin film, nanostructure

(Some figures may appear in colour only in the online journal)

Introduction

Block copolymers (BCPs) are of great interest in nanotechnology due to their ability to self-assemble into two- and three-dimensional microdomain morphologies with periods of a few nm and above [1, 2]. This length scale is beyond the resolution limit of conventional photolithography, and can be achieved by block copolymer self-assembly more economically than by direct-write methods such as electron beam lithography [3–6]. Changing the volume fraction of the blocks and the annealing conditions enables the formation of a variety of morphologies, including spheres, cylinders, double gyroid, lamellae, and perforated lamellae [7–9], which can be used to form arrays of lines, dots and other features on a substrate [10]. BCPs are particularly attractive in making arrays of high aspect ratio nanochannels [11–13], which are useful in several applications including etch masks for pattern

[5] Equal contribution.

Original content from this work may be used under the terms of the Creative Commons Attribution 3.0 licence. Any further distribution of this work must maintain attribution to the author(s) and the title of the work, journal citation and DOI.

transfer during the fabrication of memory chips, filtration membranes [14, 15], sensors [16, 17], bulk heterojunction photovoltaic cells [18], and batteries [19].

Nanofabrication based on block copolymer self-assembly typically requires control of the long range order and aspect ratio of the microdomains [20]. Previous studies have shown that chemoepitaxy and graphoepitaxy [21–29], as well as annealing under external constraints such as electric or magnetic field [30], microwave [3], shear [31], and thermal gradients [32, 33], can direct the orientation and morphology of the self-assembled microdomains. Out-of-plane orientation of cylinders or lamellae can be obtained by several methods including the use of top-coat layers [34, 35], a gradient in solvent concentration during solvent annealing [36–38], macromolecular architecture [39], or the use of chemically attractive sidewalls [23]. Exposure of BCP thin films to a solvent vapor can effectively lower the glass transition temperature, decrease polymer chain entanglement, enhance polymer diffusivity and annihilate defects, making solvent annealing an attractive alternative to thermal annealing, at ambient or at elevated [40, 41] temperatures. The final structure is produced as the film collapses in the out-of-plane direction during solvent evaporation, thus the drying process also affects the morphology [36, 37, 42]. Therefore, methods to control the microdomain morphology upon drying are desirable to preserve the ordered structure obtained during solvent annealing.

Exposure of a block copolymer film to photons or electrons can induce chemical changes, and this has been incorporated into annealing processes [43–45]. For example, holographic irradiation of a hybrid film consisting of poly (ethylene oxide)-block-poly(methacrylate derivative) with an azobenzene (Az) unit (PEO-*b*-PMMAz) and 4′-phenyl-4-cyanobiphenyl produced a corrugated relief structure [46]. UV-irradiation has been shown to lock in the self-assembled morphology of BCPs such as poly(α-methylstyrene)-block-poly(4-hydroxystyrene) (PαMS-*b*-PHOST) and polystyrene-block-poly(dimethysiloxane) (PS-*b*-PDMS) by crosslinking the exposed region, while the unexposed region can be further annealed under a different solvent vapor to change its morphology [47, 48]. Similarly, electron-beam irradiation prior to solvent vapor annealing has been used to induce local cross-linking, preventing morphology changes in the exposed regions of the BCP film [45, 49–51].

Previous studies have focused on the effect of UV exposure before or after annealing in order to stabilize the morphology, but the effect of UV exposure in the swollen state during solvent vapor annealing remains to be studied. UV irradiation can cause both cross-linking of polymer chains and an increase in temperature. Previous *in situ* observations of solvent vapor annealing found the degree of ordering reached its maximum in the swollen state and subsequent drying degraded the ordering [37]. Therefore, UV exposure during the swollen state may be able to lock in the optimum ordering by cross-linking the morphology and limiting structural collapse when the solvents are removed. This may be anticipated to produce a well-ordered self-assembled morphology with high aspect ratio microdomains.

In this article, we show how a combination of UV exposure and solvent vapor annealing can facilitate self-assembly, reduce defects, and increase the uniformity of self-assembled features in PS-*b*-PDMS BCPs. This is illustrated for both PDMS-majority and PS-majority BCPs. A particular challenge for PDMS-majority BCPs is deformation of the microdomains even in the dry state, due to the low glass transition temperature of the PDMS block. We demonstrate that UV-solvent annealing can reduce the deformation of the PDMS-majority PS-*b*-PDMS by partially crosslinking the BCP, producing a variety of well-defined morphologies in thick films including hexagonally close-packed cylinders of PS in a PDMS matrix oriented perpendicularly to the substrate. PS-*b*-PDMS was chosen because it can be treated to remove the organic PS block and convert the remaining PDMS block into a Si-rich nanostructure which can be sufficiently robust to act as a mask for subsequent pattern transfer processes [8, 52, 53].

The two PS-*b*-PDMS BCPs were: (1) a 53 kg mol^{-1} bulk-cylindrical morphology BCP with the PS block as majority [54]; and (2) a 44 kg mol^{-1} bulk-lamellar morphology with the PDMS block as majority. Although there has been extensive work on thin film morphologies of PS-majority PS-*b*-PDMS, there is little work on thin film morphologies of such a material. PDMS-majority PS-*b*-PDMS ($M_{n,PS} = 12.0$ kg mol^{-1}, $M_{n,PDMS} = 22.7$ kg mol^{-1}) has previously been prepared as 20 nm thick freestanding silicon-oxygen-carbide nanoporous membranes by forming a BCP film on a C-coated glass substrate, releasing the film by HF etching, picking it up on a TEM grid, and oxygen plasma etching [55]. Recently, PDMS-majority BCPs have been spin-coated onto various polymer and Si substrates, solvent-annealed and etched to make sub-20 nm thick porous films [56].

Materials and methods

Materials

The cylinder-forming PS-majority PS-*b*-PDMS used here (labeled SD53) has a total number average molecular weight (M_n) of 53 kg mol^{-1}, polydispersity index of 1.04, and PDMS volume fraction $f_{PS} = 0.68$. The PDMS-majority PS-*b*-PDMS used here (labeled SD44) has a PDMS volume fraction $f_{PDMS} = 0.67$, number average molecular weight of the PDMS block of 28.0 kg mol^{-1} and of the final BCP of 44.0 kg mol^{-1} (the polydispersity of the BCP was 1.06). The diblock copolymers were synthesized through anionic polymerization techniques and sequential monomer addition, following the procedures described by Bellas *et al* [57] Politakos *et al* [58] and O' Driscoll *et al* [59]. The molecular characteristics were calculated and verified by size exclusion chromotagraphy, membrane osmometry and proton nuclear magnetic resonance (^{1}H-NMR) spectroscopy. Homopolymers of PS ($M_n = 10$ kg mol^{-1}, $M_w/M_n = 1.2$) and PDMS ($M_n = 5.5$ kg mol^{-1}, $M_w/M_n = 1.2$) were obtained from Polymer Source, Inc.

Film fabrication and characterization

SD53 and SD44 were dissolved into 1 wt% cyclohexane and 5 wt% toluene solution, respectively and spin-coated onto silicon substrates (5000 rpm) or template substrates (3000 rpm). After solvent vapor annealing of the resulting thin films (with or without UV post-annealing exposure), the samples were treated first with 5s CF_4/O_2 plasma etch at 50 W and then 22s O_2 plasma etch at 90 W in order to remove PS and reveal the self-assembled microdomain morphology. The film thickness was measured by a Filmetrics F20 spectral reflectometer. The bulk morphology of SD44 was measured in a 3 μm thick sample prepared by drop-casting on a silicon substrate from 5 wt% toluene solution, slow drying, annealing in a vacuum oven at 150 °C at a pressure of 20 Torr for 48 h and then etching. The morphology of the films was revealed through scanning electron microscopy (SEM, Zeiss MERLIN, SEM, acceleration voltage 5 kV, inLens detector). All samples were sputtered with a 2–3 nm thick Au–Pt layer before SEM imaging in order to minimize charging effects. A TA Instruments Q20 Differential Scanning Calorimeter was used to determine the glass transition temperature.

Solvent annealing

The SD53 films were solvent vapor annealed in a small glass chamber (volume 50 cm^3) containing 1.5 ml of a liquid solvent mixture. The SD44 thin films were placed into a larger 84 cm^3 glass annealing chamber with 20 ml of a liquid solvent mixture such as a toluene and heptane. In both cases the sample was supported above the liquid surface within the annealing chamber. The samples were quenched by rapidly opening the lid of the annealing chamber, and the film deswelled to its original thickness within seconds. For UV-assisted solvent vapor annealing, a quartz cover, which transmits 90% of UV light at 254 nm, was used to cover the annealing chamber [60]. The total annealing time for SD53 films is 60 min, and for SD44 films is 100 min.

We used a solvent vapor generated from a toluene: heptane x:1 volumetric mixture for solvent annealing, where $x = 5$, 2, 1 or 1/3. Several annealing procedures were also carried out in acetone vapor. The estimated partial pressure corresponding to the solvent mixture is given in the supplementary material, table S1. Figure S3 shows swelling of SD44 and homopolymers in vapor from a 1:1 toluene:heptane mixture.

UV irradiation was carried out using a XX-115S Shortwave UV Bench Lamp with power of 15 W. This is a mercury lamp with strong emission at 254 nm (ultraviolet UVC) and 365 nm (i-line) wavelengths, and was placed 20 cm above the samples. The power density at 20 cm distance was typically around 3.0 mW cm^{-2}. Although PDMS is not highly absorbent in the UV range, it can still be effectively cross-linked by UV, forming hydroxyl and silicon oxide groups on the surface [61]. Another study showed that UV irradiation with a power density of 19.0 mW cm^{-2} for 6 h is able to crosslink a PS thin film [62], while excessive exposure may lead to polymer degradation [63]. Therefore, although both blocks are cross-linkable by UV, the major effect of the UV is to reduce the solubility in solvent of the PDMS block, as described below. Figure S4 shows the prcess flow.

Substrate patterning

The gratings were fabricated using a Lloyd's Mirror Interference Lithography system [64], which uses the intersection of two coherent laser beams in order to create a periodic intensity pattern of light to expose a resist. To make high aspect-ratio trenches, a tri-layer resist stack consisting of 200 nm PFI 88 negative photoresist layer on top, 20 nm SiO_2 layer, and 450 nm anti-reflective coating (ARC) were deposited on a silicon substrate. A helium–cadmium laser emitting at 325 nm was used to expose a grating pattern. After exposure and development of the resist, the grating pattern was transferred into the silica, then into the ARC layer using reactive ion etching (RIE) to produce trenches with approximately vertical ARC sidewalls. To functionalize the trench surface with a thin layer of PDMS brush, a layer of hydroxyl-terminated PDMS ($M_n = 0.8$ kg mol^{-1}) was spin-coated from a 5 wt% toluene solution, vacuum-baked at 20 Torr, 170 °C for 14 h, and then rinsed in toluene.

Two-step grating substrates were fabricated in a similar manner except that the ARC was 200 nm thick. After exposure and development, the grating pattern was transferred from the photoresist layer into the Si substrate using RIE. Part of the ARC remained at the center of the mesas of the silica trench pattern, forming lines 30 nm thick. This led to a two-step trench topography, figure S1.

Results and discussion

Effect of UV exposure on SD53 swelling ratio

The optical absorbance (logarithm of (incident radiant flux/transmitted radiant flux)) of an 80 nm thick SD53 film on a Si substrate is shown in figure S1 indicating strong absorbance at 250–300 nm wavelengths, though the polymer was mostly transparent to the i-line peak at 365 nm. Therefore the BCPs as well as the toluene and heptane [65] solvent vapors can absorb at least part of the output of the UV mercury lamp.

The effect of UV irradiation on 80 nm thick PS homopolymer (hPS), PDMS homopolymer (hPDMS), and SD53 was first tested by measuring the film thickness change after films were irradiated and then immersed in liquid toluene for 1 min. Without UV irradiation, the 1 min immersion in toluene completely dissolved all hPS, hPDMS, and SD53 films. However after 20 min UV irradiation (total dose around 450 mJ cm^{-2}) the measured dried film thickness, after immersion into liquid toluene for hPS was ~10 nm, for PDMS ~70 nm, and for SD53 ~50 nm. This suggests that the 20 min UV exposure induced cross-linking of hPS, hPDMS and SD53 films, with the greatest resistance to dissolution found in the hPDMS and the least in the hPS. In subsequent experiments, 5 min of UV irradiation was chosen in order to

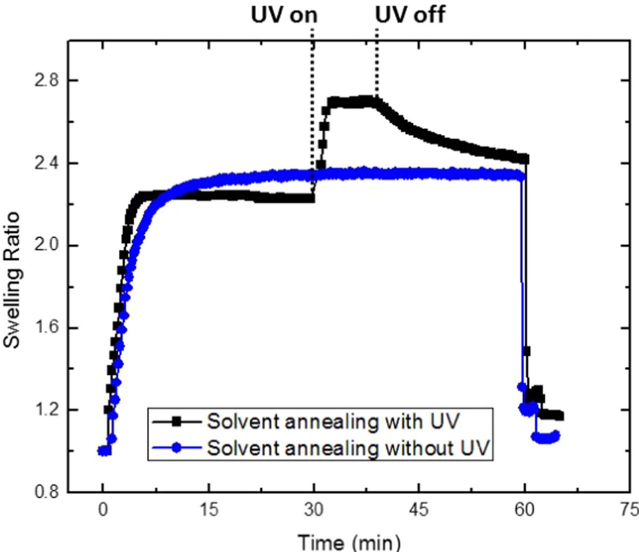

Figure 1. Swelling ratio data versus time during solvent vapor annealing. The SD53 films had an as-spun thickness of 80 nm and were annealed in a chamber with a vapor from a mixture of toluene: heptane 5:1 volumetric ratio. Both films initially swelled to 2.4 times the starting thickness. The introduction of UV light caused a swelling increase over about 2 min, followed by a slow deswelling after the UV light was turned off.

only partially crosslink the PS-*b*-PDMS BCP in the swelled state.

The effect of UV irradiation on the swelling behavior of PS-*b*-PDMS film was tested by *in situ* measurement of the swelling ratio of SD53 films with as-cast thickness 80 nm (figure 1). The solvent vapor composition was chosen based on a previous study [37] where it was concluded that the solvent vapors generated from a 5:1 volumetric mixture produced approximately equal swelling of the PS and PDMS blocks of a bulk cylinder-forming PS-*b*-PDMS BCP, ensuring that the cylindrical morphology forms at the swelled state in the thin film. (It should be noted, however, that crosslinking of the blocks will affect the relative solvent uptake rendering the 5:1 solvent ratio more preferential to swelling the PS blocks.) Without UV irradiation, SD53 films showed a swelling ratio of 2.2–2.3, but when the UV was switched on the swelling ratio of the film increased to 2.6 over ~2 min.

Effect of UV irradiation on PS-majority SD53 thin film morphology during solvent-annealing

We first describe the morphology of as-cast SD53 films of different thickness at a saturated swelling ratio of around 2.25, using the vapor from a toluene:heptane 5:1 volumetric ratio. An as-deposited film with thickness 36 nm exhibited micelle-like morphology (figure 2(a)) with period 37 nm. After 1 h solvent annealing without UV irradiation, a SD53 film with 25 nm as-cast thickness produced discontinuous cylinders with poor ordering (figure 2(b)); a 36 nm film formed continuous cylinders with a low correlation length and period 33 nm (figure 2(c)); and a 78 nm film produced double-layer cylinders with breaks in the top-layer cylinders (figure 2(d)). The commensurability between the SD53 film thickness and the natural periodicity of SD53 is an important factor in improving the degree of ordering of the self-assembled morphology [7, 68]. Comparing figures 2(b)–(d), 36 nm as-cast thickness appears to be closest to the commensurate condition under the annealing conditions of the experiment, therefore, the as-cast thickness was fixed at 36 nm and films were treated with UV irradiation during different stages of the solvent annealing.

When UV irradiation was performed on a 36 nm thick film without solvent vapor annealing, the film morphology was similar to the as-cast morphology. The film formed micelles with period 32 nm (figure 2(e)) although the PDMS area ratio became smaller, and the initiation of micelles merging into short cylinders was evident. However, UV irradiation of a swelled film within the first 5 min of solvent vapor annealing produced a mixture of cylinders having different lengths (figure 2(f)). This suggests that partial crosslinking limited the diffusivity during subsequent solvent vapor exposure.

In contrast, UV irradiation during the last 5 min of solvent annealing led to well-ordered cylindrical morphologies in SD53 films with both 36 nm and 80 nm as-cast thickness, with average microdomain grain size around 8 μm^2 and 1 μm^2 respectively (figures 2(g) and (h)). This can be compared with the average grain size of samples solvent-annealed with no UV irradiation (figures 2(c) and (d)), which was 10^{-2} μm^2 and 5×10^{-3} μm^2, respectively. (The average grain sizes were estimated based on mapping the grain boundaries from several SEM images using ImageJ software and calculating the grain areas). The ordering improvement is most evident for the commensurate film thickness, 36 nm, but still appeared for the 80 nm thick film. The observations suggest that UV irradiation can lock in the self-assembled morphology of the swelled state, limiting degradation of the ordering induced by deswelling. The period of the UV-annealed morphology of the 36 nm film in figure 2(g) is 34 nm compared to 32 nm in figure 2(c). An *in situ* study of the solvent vapor annealing of a cylinder-forming PS-PDMS film confirmed that deswelling induces the collapse of the self-assembled lattice structure [69]. The larger period for the UV-solvent annealed sample suggests that UV-induced crosslinking in the swelled state decreased the degree of shrinkage during deswelling.

Compared with non-UV solvent-annealed samples, the improvement of ordering in UV solvent-annealed samples is attributed to two factors: (i) the UV irradiation induced a raise of temperature of the solvent annealing system, thus increasing the solvent vapor pressure and swelling ratio of the sample; (ii) the UV irradiation partially crosslinked the swelled polymer chains, locked in the self-assembled morphology, and minimized the deformation of microdomains during film deswelling. The UV light raised the temperature in the chamber by 3 °C on average, according to a thermocouple suspended in the chamber (the surface temperature of the substrate may have been higher). Heating the solvent reservoir leads to a higher solvent vapor partial pressure (e.g. a 3 °C temperature change at 20 °C would raise

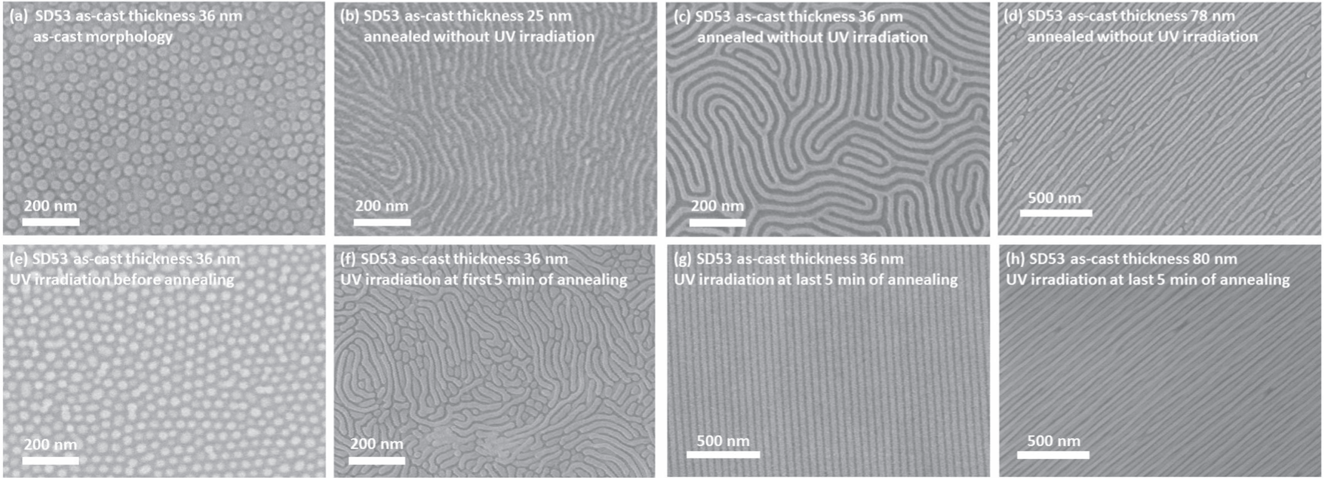

Figure 2. Representative SEM images of oxidized PDMS microdomains formed from solvent annealed SD53 thin films with differing as-cast thickness. Samples were processed by solvent vapor annealing with solvent vapors generated from a reservoir of toluene: heptane 5:1 volumetric mixture for 1 h. (a) As-cast morphology; (b) annealed without UV irradiation; (c) annealed without UV irradiation; (d) annealed without UV irradiation; (e) 5 min UV irradiation before annealing; (f) UV irradiation during first 5 min of annealing; (g) UV irradiation during last 5 min of annealing; (h) UV irradiation during last 5 min of annealing. As-cast film thickness: (a) 36 nm; (b) 25 nm; (c) 36 nm; (d) 78 nm; (e) 36 nm; (f) 36 nm; (g) 36 nm; (h) 80 nm.

the vapor pressure of toluene by a factor 1.17 based on its heat of evaporation) which would increase the swelling ratio. The film deswelled and cooled when the light was turned off but did not return to its former swelling ratio by the end of the 60 min anneal, assumed to be a result of cross-linking based on the comparison with the swelling behavior of non-UV solvent annealing (figure 1). A previous study showed that heating the sample (but not the chamber) drove the solvent out of the BCP film and led to deswelling [41], whereas other work showed that heating the entire chamber resulted in an increase in the solvent vapor pressure, which increased the solvent uptake [66, 67]. Our work is more closely related to the latter cases since the UV lamp heated the vapors and the chamber as well as the sample. Increased swelling has been shown to improve the degree of ordering [37].

Film morphology of PDMS-majority SD44 films after UV-solvent vapor annealing

The bulk morphology of SD44 consisted of lamellae with a period of 50 nm corresponding to PS and PDMS layer thicknesses of approximately 13 nm and 37 nm, respectively (figure 3(a)). Lamellae formed rather than cylinders despite the deviation of the volume fraction from 0.5 ($f_{PDMS} = 0.67$ for SD44). DSC measurements of SD44 (figure 3(b)) showed a melting temperature of the majority component (PDMS) at -40 °C and a glass transition temperature of the minority component, PS, at 96 °C (± 3 °C). Homopolymers, hPDMS and hPS, exhibit glass transition temperatures of -125 °C and 107 °C [70, 71] respectively and the melting temperature of crystalline hPDMS is reported around -40 °C. The most notable difference between SD44 and SD53 films was the distortion of microdomains that occurred even after drying in solvent-annealed SD44 films prepared without UV irradiation, exemplified in figure 3(d). This is caused by the viscoelastic behavior of the majority PDMS block, and presents a processing challenge for such materials not present in PS-majority BCPs. In this section we show that the cross-linking induced by UV irradiation made the self-assembled nanostructure more robust (figure 3(f)) and enabled formation of a through-thickness pore array.

In order to produce a cylindrical morphology by solvent annealing, the solvent vapor was generated from a toluene: heptane 1:1 volumetric mixture (figure S3) instead of the 5:1 mixture used in the SD53. The increased heptane fraction drives the morphology from lamellae towards PS cylinders. Annealing was carried out for 100 min at a saturated swelling ratio of 2.75 for a 180 nm thick film (figure 3(c)). This led to a PS cylinder morphology with center-to-center periodicity of 44 nm and hole diameter of ~14 nm after etching. The effects of different solvent vapor compositions on morphology will be described below. CF_4/O_2 and O_2 plasma etching showed that the top surface of the etched film consisted of oxidized PDMS with an array of holes (figures 3(d) and (e)).

Although the solvent-annealed SD44 showed a pore array at its top surface, a cross-sectional image, prepared by cooling the sample in liquid nitrogen for 20 s, cracking it using a diamond scriber and etching it, did not show the pores penetrating vertically throughout the thickness of the film (figure 3(d)). This behavior was attributed to deformation of the low glass transition temperature majority PDMS block, even in the dry state. The etching process oxidized only the top layer of the film, and the interior of the film was able to deform during the preparation of the cross-section.

Unlike a PS-majority BCP, which has a stable morphology at room temperature, the PDMS-majority BCP is apparently able to deform even in the dry state at room temperature which limits its utility as a nanochannel film or a pattern transfer mask. To stabilize the microphase-separated structure, 5 min UV exposure at intensity ~3 mW cm^{-2} was

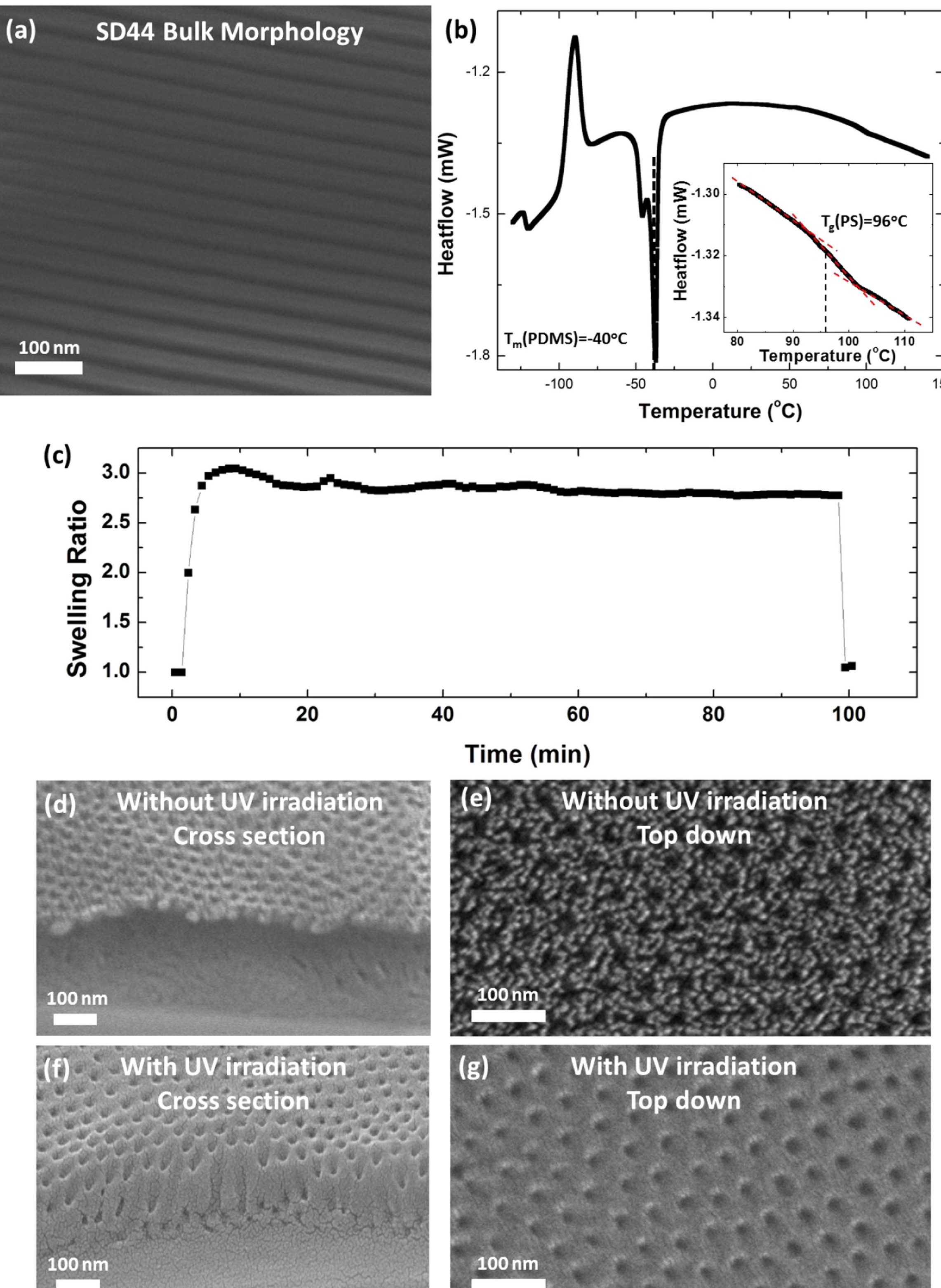

Figure 3. Self-assembly of SD44 PS-*b*-PDMS BCP. (a) SEM of the bulk lamellar morphology. The sample was thermally annealed in a vacuum oven at 150 °C at a pressure of 20 Torr for 48 h. PDMS microdomains appear brighter. (b) Differential scanning calorimetry measurement of SD44. The glass transition temperature for the PS block was observed at 96 °C (inset). The melting temperature for the PDMS block was observed at −40 °C. (c) *In situ* swelling ratio measurement of SD44 film under solvent vapor from a toluene: heptane 1:1 volumetric mixture. The as-cast thickness of the SD44 film was 180 nm. (d), (e), SEM of 180 nm thick SD44 film annealed at room temperature in a solvent vapor generated by a toluene: heptane 1:1 mixture for 1.5 h, followed by reactive ion etching. (d) Cross-section view, (e) top-down view. (f), (g), a film processed in the same way as shown in (d) but exposed to UV light for 5 min before drying and etching. (f) Cross-section view, (g) top-down view.

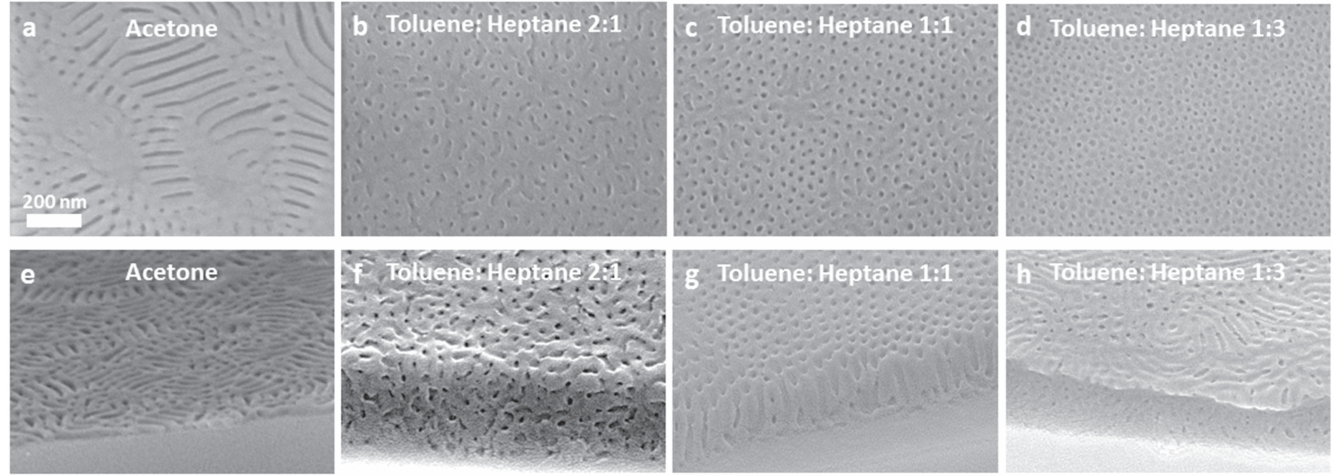

Figure 4. The effect of solvent composition on the morphology of SD44 films. The swelled films were exposed to 5 min UV prior to deswelling. (a), (e) SD44 thin film with as-cast thickness 100 nm annealed under acetone vapors for 1.5 h, (a) top-down view, (e) cross-section view; (b), (f) SD44 thin film with as-cast thickness 200 nm annealed under solvent vapors generated by toluene: heptane 2:1 volumetric mixture for 1.5 h, (b) top-down view, (f) cross-section view; (c), (g) SD44 thin film with as-cast thickness 180 nm annealed under solvent vapors generated by toluene: heptane 1:1 mixture for 1.5 h as in figures 3(f) and (g); (c) top-down view, (g) cross-section view; (d), (h) SD44 thin film with as-cast thickness 160 nm annealed under solvent vapors generated by toluene: heptane 1:3 mixture (d) top-down view, (h) crosssection view.

applied to the film before deswelling (see process of figures 2(f)–(h)), in order to partially cross-link the polymer. Figures 3(f) and (g) shows the cross-section and top-view morphology of the SD44 film prepared in the same way as figures 3(d) and (e) respectively, with the only exception being the use of 5 min UV. The UV-processed film showed pores penetrating the film thickness, although the cross-section cut through some of the pores at an angle. (The granularity in figure 3(e) arises from the metal coating, but the array of pores is clearly visible.)

The orientation of the cylinders is affected by both the annealing process and the surface energies of the blocks. For PS-*b*-PDMS, a PDMS wetting layer is usually formed at the air/film interface due to the lower surface energy of PDMS (in the swollen state, the interfacial tension of PS with air is 32.1 mN m^{-1} at room temperature, whereas PDMS with air is 20.9 mN m^{-1}) [35, 72]. This PDMS wetting layer promotes an in-plane cylinder orientation. However, an out-of-plane orientation can form instead as a result of solvent concentration gradients, especially in thicker films. An *in situ* study showed a time-dependent cylinder orientation in which the cylinders were initially out-of-plane, but reoriented towards the in-plane direction during solvent vapor annealing [37]. In the present work, we conclude that the combination of film thickness and the solvent vapor annealing led to the out-of-plane cylinders seen in figure 3(d).

Effect of solvent vapor composition on UV-solvent annealed SD44 thin film morphology

By varying the solvent or solvent mixture used in the UV-solvent vapor annealing process and therefore the selectivity of the solvent to the two blocks, a wide range of rigid, high aspect ratio self-assembled nanostructures was produced. The morphology transitions are a result of the different affinities of toluene and heptane towards PS and PDMS blocks which changes the effective volume fraction due to their asymmetric swelling [8]. For example, the vapor produced from the 1:1 toluene:heptane mixture caused a swelling ratio of 3.5 for hPS, 2.3 for hPDMS films, and 2.75 for the SD44.

A lamellar morphology was found in a SD44 film with 100 nm as-cast thickness after annealing under acetone vapor (figures 4(a) and (e)). Acetone has a solubility parameter of 19.7 $MPa^{1/2}$, which is closer to that of PS (18.5 $MPa^{1/2}$) than that of PDMS (15.5 $MPa^{1/2}$), thus it is expected to swell PS more, driving the effective volume fraction towards that of a lamellar phase. The out-of-plane orientation of the SD44 lamellae annealed by acetone is attributed to the solvent concentration gradient through the film [35, 37, 73], similar to the formation of vertical PS cylinders in toluene:heptane vapors in figure 3. The top surface of the film has a PDMS wetting layer which is only partly removed in figure 4(a).

A 200 nm thick film annealed in vapor generated by a toluene: heptane 2:1 volumetric mixture (figures 4(b) and (f)) exhibited a porous morphology with poorly ordered, narrow pores. Cylindrical channels oriented out-of-plane were formed in a 180 nm thick film annealed in solvent vapor generated by a toluene: heptane 1:1 mixture, as described in the previous section (figures 3(d), (e) and 4(c), (g)). A mixed morphology containing spheres and cylinders of polystyrene was formed from a 160 nm film annealed in vapor from a toluene: heptane 1:3 mixture (figures 4(d) and (h)). Therefore, increasing the helptane fraction led to morphologies with a qualitatively lower volume fraction of PS; the period of the morphology also decreased from ~45 to ~33 nm with increasing heptane. The structures are less well ordered than those seen in figure 2 for monolayer SD53, but they do illustrate that a range of morphologies including vertical lamellae is enabled by changing the solvent composition. Control of morphology has been reported previously in PS-majority PS-*b*-PDMS BCPs [1, 6, 7].

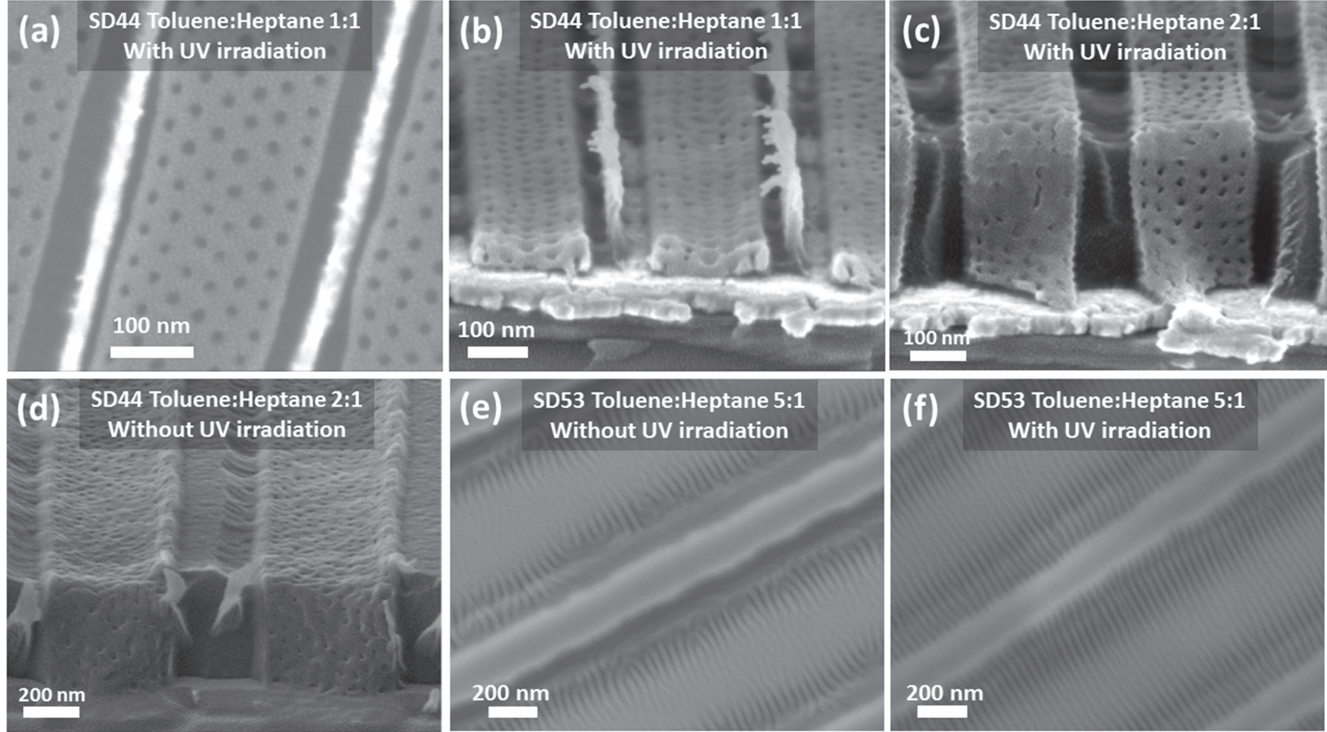

Figure 5. Directed self-assembly of SD44 films and SD53 films. (SD44 films on high aspect-ratio trenches and SD53 films on two-step trenches.) (a) (b) SD44 thin film with as-cast thickness 80 nm was annealed under solvent vapor generated by toluene: heptane 1:1 reservoir mixture for 1.5 h. (a) Top-down view, (b) cross-section view. The fins are residues of the mesas of the grating pattern. (c) SD44 thin film with as-cast thickness 280 nm was annealed under solvent vapor generated by toluene: heptane 2:1 reservoir mixture for 1.5 h with UV irradiation during the last 5 min of annealing. (d) SD44 thin film with as-cast thickness 250 nm was annealed under solvent vapor generated by toluene: heptane 2:1 reservoir mixture for 1.5 h without UV irradiation. Trench height 300 nm; trench width (a)–(c) 200 nm; (d) 450 nm. (e) SD53 film solvent-annealed under solvent vapors from toluene heptane 5:1 volumetric mixture without UV irradiation, showing poorly-ordered in-plane cylinders; (f) SD53 film UV-assisted solvent annealed from toluene heptane 5:1 volumetric mixture with UV irradiation during the last 5 min of annealing, showing well-ordered in-plane cylinders.

Directed self-assembly of SD53 and SD44 films by UV-assisted solvent vapor annealing

The correlation length of the SD44 pore arrays in figures 3(g), and 4(c) is limited to a few periods, but templating the microphase separation using topographical features is expected to improve the ordering [23]. High aspect-ratio gratings (figures 5(a)–(c), trench height 300 nm, width 200 nm; figure 5(d), trench height 300 nm, width 450 nm) were patterned by a Lloyd's Mirror interference lithography system [64], in which the intersection of two mutually coherent laser beams creates a periodic intensity pattern of light which exposes a resist with a grating pattern. The SD44 was spin-coated onto the PDMS-functionalized gratings, solvent annealed in toluene:heptane vapor, with UV exposure before deswelling, and etched in oxygen plasma.

The templating by the narrower trenches produced an ordered arrangement of out-of-plane channels in the etched BCP, with PDMS wetting the sidewalls. Figures 5(a) and (b) shows results using vapor from a toluene: heptane 1:1 mixture. For an 80 nm thick film (figure 5(a)), a well-ordered close-packed array formed in the trench with rows of cylinders parallel to the trench edges. The vertical fins are remnants of the ARC used to form the trench edges. The center-to-center distance between each hole is 36 nm and the hole diameter is around 14 nm. The center-to-center distance was ~8 nm smaller than the untemplated morphology (figure 3(e)), a behavior which may be attributed to the physical confinement provided by the trench as well as the surface energy of the trench sidewall that induced preferential wetting by PDMS. Incommensurability between the trench width and the BCP row spacing led to a reduction in period such that six rows of cylinders (unconfined row spacing = 38 nm) could fit within a 200 nm wide trench (confined row spacing = 33 nm).

Figures 5(c) and (d) show results of templated assembly of SD44 after annealing in vapor from a toluene: heptane 2:1 mixture, using the same solvent anneal condition as was used for smooth substrates (figure 4(b)). Figure 5(c) included UV irradiation in the last 5 min of solvent annealing while figure 5(d) was processed without UV irradiation. The sample of figure 5(d) had a wider trench width and exhibited a disordered porous structure, deformed by the flow of the PDMS block. However, the grating template with narrower trenches in figure 5(c) produced what appears to be a perforated lamellar structure in which adjacent PDMS lamellae appear to be interconnected through pores in the PS lamellae, and the ordering of the structure is preserved by UV crosslinking. The 200 nm wide trenches of figure 5(c) each contained seven PDMS lamellae and six PS perforated lamellae implying a

~15% smaller period than that of the drop-cast bulk BCP, similar to the confinement-induced reduction in period seen in figures 5(a) and (b).

Previous studies of cylindrical morphology PS-*b*-PDMS with minority PDMS used trenches with vertical sidewalls and produced in-plane cylinders parallel or perpendicular to the trench walls depending on the annealing process [54]. To examine directed self-assembly of SD53 we used two-step trenches to facilitate flow of the swollen polymer towards the middle of the trench and to promote the formation of in-plane cylinders oriented perpendicular to the trenches [21]. An SEM image of the trench is shown in figure S2.

When a 36 nm thick film of SD53 was spin coated, the film formed in-plane cylinders in a fingerprint pattern independent of the trench structure, rather than the micelles that were observed on the bare Si substrate. After solvent annealing in 5:1 toluene: heptane, the cylinders were contained between and largely perpendicular to the lower trench wall (figure 5(e)), as expected [21]. When UV solvent annealing was used, however, the orientation and periodicity of the cylinders was improved (figure 5(f)) from ~35% of cylinders aligned perpendicular to the trenches in non-UV solvent vapor annealing to 93% in UV solvent vapor annealing. Therefore, directed self-assembly can be combined with UV-assisted solvent annealing to produce both PS-majority and PDMS-majority BCP films with well-ordered 3D microdomain structures.

Conclusion

The influence of UV irradiation on the self-assembly of both PS-majority and PDMS-majority PS-*b*-PDMS films was investigated, with the particular aim of stabilizing the microdomain structure of PDMS-majority films which is subject to distortion even in the dry state as a result of the low glass transition temperature of PDMS. UV exposure in the swelled state at the end of the solvent annealing process was effective in partially cross-linking the BCP, which preserved the microdomain structure formed by the solvent anneal. UV exposure also led to an increase in temperature of the annealing chamber which increased the vapor pressure of solvents and the swelling of the films. The UV exposure led in some cases to final microdomain morphologies, i.e. cylinders in the SD53 ($f_{PDMS} = 0.32$) film and nanochannels in the SD44 ($f_{PDMS} = 0.67$) film, with better order than those obtained from just a solvent annealing procedure.

The influence of solvent vapor composition on the morphology of the SD44 was further investigated. In bulk the SD44 formed a lamellar morphology but thin films produced a diversity of structures depending on the solvent vapor composition: acetone or toluene-heptane mixtures. These included disordered porous structures and cylinders or lamellae oriented perpendicular to the substrate. Films of SD44 coated onto grating substrates consisting of high aspect-ratio trenches showed enhanced ordering of pores, and a perforated lamellar structure under certain annealing conditions, whereas SD53 coated on grating structures showed in-plane alignment of PDMS cylinders perpendicular to the sidewalls. The perpendicular nanochannel arrays formed from the SD44 PDMS-majority BCP may be useful in pattern transfer for nanolithography as well as other applications such as filtration membranes and sensors. The UV-assisted solvent vapor annealing is extendable to other BCP systems that are susceptible to cross-linking, and thus could provide a simple tool to improve the quality of self-assembled thin films.

Acknowledgments

We are grateful for discussion with Dr Adam Hannon of National Institute of Standards and Technology, Gaithersburg, and for technical assistance from Dr Geetha Berera and Alan Schwartzman of MIT. The support of Samsung Electronics is gratefully acknowledged. TH acknowledges support from Tokyo Institute of Technology. Shared experimental facilities of CMSE, award NSF DMR1419807, and the Nanostructures Laboratory, MTL were used.

References

[1] Jung Y S and Ross C A 2009 Solvent-vapor-induced tunability of self-assembled block copolymer patterns *Adv. Mater.* **21** 2540–5
[2] Choi H K, Gwyther J, Manners I and Ross C A 2012 Square arrays of holes and dots patterned from a linear ABC triblock terpolymer *ACS Nano* **6** 8342–8
[3] Zhang X, Harris K D, Wu N L Y, Murphy J N and Buriak J M 2010 Fast assembly of ordered block copolymer nanostructures through microwave annealing *ACS Nano* **4** 7021–9
[4] Kim S, Nealey P F and Bates F S 2014 Directed assembly of lamellae forming block copolymer thin films near the order-disorder transition *Nano Lett.* **14** 148–52
[5] Mansky P, Haikin P and Thomas E L 1995 Monolayer films of diblock copolymer microdomains for nanolithographic applications *J. Mater. Sci.* **30** 1987–92
[6] Wang Z, Li T, Schulte L, Almdal K and Ndoni S 2016 Photocatalytic nanostructuring of graphene guided by block copolymer self-assembly *ACS Appl. Mater. Interfaces* **8** 8329–34
[7] Bai W, Hannon A F, Gotrik K W, Choi H K, Aissou K, Liontos G, Ntetsikas K, Alexander-Katz A, Avgeropoulos A and Ross C A 2014 Thin film morphologies of bulk-gyroid polystyrene- block -polydimethylsiloxane under solvent vapor annealing *Macromolecules* **47** 6000–8
[8] Gotrik K W, Hannon A F, Son J G, Keller B, Alexander-Katz A and Ross C A 2012 Morphology control in block copolymer films using mixed solvent vapors *ACS Nano* **6** 8052–9
[9] Lo T-Y, Ho R-M, Georgopanos P, Avgeropoulos A and Hashimoto T 2013 Direct visualization of order–order transitions in silicon-containing block copolymers by electron tomography *ACS Macro Lett.* **2** 190–4
[10] Park W I, Choi Y J, Yun J M, Hong S W, Jung Y S and Kim K H 2015 Enhancing the directed self-assembly kinetics of block copolymers using binary solvent mixtures *ACS Appl. Mater. Interfaces* **7** 25843–50

[11] Schacher F H, Rupar P A and Manners I 2012 Functional block copolymers: nanostructured materials with emerging applications *Angew. Chem., Int. Ed. Engl.* **51** 7898–921
[12] Hamley I W 2003 Nanostructure fabrication using block copolymers *Nanotechnology* **14** R39–54
[13] Segalman R A 2005 Patterning with block copolymer thin films *Mater. Sci. Eng.* R **48** 191–226
[14] Jackson E A and Hillmyer M A 2010 Nanoporous membranes derived from block copolymers: from drug delivery to water filtration *ACS Nano* **4** 3548–53
[15] Liu Y, Wang W, Wu W, Yang F and Li H 2015 Filtration membrane with ultra-high porosity and pore size controllability fabricated by parylene c molding technique for targeted cell separation from bronchoalveolar lavage fluid (BALF) *2015 Transducers— 18th Int. Conf. on Solid-State Sensors, Actuators and Microsystems (TRANSDUCERS)* pp 1767–9
[16] Jeong C K, Jin H M, Ahn J-H, Park T J, Yoo H G, Koo M, Choi Y-K, Kim S O and Lee K J 2014 Biosensors: electrical biomolecule detection using nanopatterned silicon via block copolymer lithography *Small* **10** 213
[17] Wagner T, Haffer S, Weinberger C, Klaus D and Tiemann M 2013 Mesoporous materials as gas sensors *Chem. Soc. Rev.* **42** 4036–53
[18] Tao Y, McCulloch B, Kim S and Segalman R A 2009 The relationship between morphology and performance of donor–acceptor rod–coil block copolymer solar cells *Soft Matter* **5** 4219
[19] Orilall M C and Wiesner U 2011 Block copolymer based composition and morphology control in nanostructured hybrid materials for energy conversion and storage: solar cells, batteries, and fuel cells *Chem. Soc. Rev.* **40** 520–35
[20] Sinturel C, Vayer M, Morris M and Hillmyer M A 2013 Solvent vapor annealing of block polymer thin films *Macromolecules* **46** 5399–415
[21] Jung Y S and Ross C A 2007 Orientation-controlled self-assembled nanolithography using a polystyrene—polydimethylsiloxane block copolymer *Nano Lett.* **7** 2046–50
[22] Park S, Tsarkova L, Hiltl S, Roitsch S, Mayer J and Böker A 2012 Guiding block copolymers into sequenced patterns via inverted terrace formation *Macromolecules* **45** 2494–501
[23] Bai W, Gadelrab K, Alexander-Katz A and Ross C A 2015 Perpendicular block copolymer microdomains in high aspect ratio templates *Nano Lett.* **15** 6901–8
[24] Cheng J Y, Mayes A M and Ross C A 2004 Nanostructure engineering by templated self-assembly of block copolymers *Nat. Mater.* **3** 823–8
[25] Darling S B 2007 Directing the self-assembly of block copolymers *Prog. Polym. Sci.* **32** 1152–204
[26] Kim S O, Solak H H, Stoykovich M P, Ferrier N J, De Pablo J J and Nealey P F 2003 Epitaxial self-assembly of block copolymers on lithographically defined nanopatterned substrates *Nature* **424** 411–4
[27] Luo M and Epps T H 2013 Directed block copolymer thin film self-assembly: emerging trends in nanopattern fabrication *Macromolecules* **46** 7567–79
[28] Segalman R A, Yokoyama H and Kramer E J 2001 Graphoepitaxy of spherical domain block copolymer films *Adv. Mater.* **13** 1152–5
[29] Borah D, Rasappa S, Salaun M, Zellsman M, Lorret O, Liontos G, Ntetsikas K, Avgeropoulos A and Morris M A 2015 Soft graphoepitaxy for large area directed self-assembly of polystyrene-*block*-poly(dimethylsiloxane) block copolymer on nanopatterned POSS substrates fabricated by nanoimprint lithography *Adv. Funct. Mater.* **25** 3425–32
[30] Olszowka V, Hund M, Kuntermann V, Scherdel S, Tsarkova L and Böker A 2009 Electric field alignment of a block copolymer nanopattern: direct observation of the microscopic mechanism *ACS Nano* **3** 1091–6
[31] Angelescu D E, Waller J H, Adamson D H, Deshpande P, Chou S Y, Register R A and Chaikin P M 2004 Macroscopic orientation of block copolymer cylinders in single-layer films by shearing *Adv. Mater.* **16** 1736–40
[32] Majewski P W and Yager K G 2015 Millisecond ordering of block copolymer films via photothermal gradients *ACS Nano* **9** 3896–906
[33] Singer J P, Lin P-T, Kooi S E, Kimerling L C, Michel J and Thomas E L 2013 Direct-write thermocapillary dewetting of polymer thin films by a laser-induced thermal gradient *Adv. Mater.* **25** 6100–5
[34] Bates C M, Seshimo T, Maher M J, Durand W J, Cushen J D, Dean L M, Blachut G, Ellison C J and Willson C G 2012 Polarity-switching top coats enable orientation of sub-10 nm block copolymer domains *Science* **338** 775–9
[35] Kim E, Kim W, Lee K H, Ross C A and Son J G 2014 A top coat with solvent annealing enables perpendicular orientation of sub-10 nm microdomains in Si-containing block copolymer thin films *Adv. Funct. Mater.* 6981–8
[36] Son J G, Gotrik K W and Ross C A 2012 High-aspect-ratio perpendicular orientation of PS- B -PDMS thin films under solvent annealing *ACS Macro Lett.* **1** 1279–84
[37] Bai W, Yager K G and Ross C A 2015 *In situ* characterization of the self-assembly of a polystyrene–polydimethylsiloxane block copolymer during solvent vapor annealing *Macromolecules* **48** 8574–84
[38] Cavicchi K A and Russell T P 2007 Solvent annealed thin films of asymmetric polyisoprene−polylactide diblock copolymers *Macromolecules* **40** 1181–6
[39] Lo T-Y, Dehghan A, Georgopanos P, Avgeropoulos A, Shi A-C and Ho R-M 2016 Orienting block copolymer thin films via entropy *Macromolecules* **49** 624–33
[40] Lee J H, Kim Y, Cho J-Y, Yang S R, Kim J M, Yim S, Lee H and Jung Y S 2015 *In situ* nanolithography with sub-10 nm resolution realized by thermally assisted spin-casting of a self-assembling polymer *Adv. Mater.* **27** 4814–22
[41] Gotrik K W and Ross C A 2013 Solvothermal annealing of block copolymer thin films *Nano Lett.* **13** 5117–22
[42] Phillip W A, Hillmyer M A and Cussler E L 2010 Cylinder orientation mechanism in block copolymer thin films upon solvent evaporation *Macromolecules* **43** 7763–70
[43] He C and Stoykovich M P 2015 Photopatterning of cross-linkable epoxide-functionalized block copolymers and dual-tone nanostructure development for fabrication across the nano- and microscales *Small* **11** 2407–16
[44] Singer J P, Gotrik K W, Lee J-H, Kooi S E, Ross C A and Thomas E L 2014 Alignment and reordering of a block copolymer by solvent-enhanced thermal laser direct write *Polymer (Guildf)* **55** 1875–82
[45] Son J G, Chang J-B, Berggren K K and Ross C A 2011 Assembly of sub-10 nm block copolymer patterns with mixed morphology and period using electron irradiation and solvent annealing *Nano Lett.* **11** 5079–84
[46] Morikawa Y, Nagano S, Watanabe K, Kamata K, Iyoda T and Seki T 2006 Optical alignment and patterning of nanoscale microdomains in a block copolymer thin film *Adv. Mater.* **18** 883–6
[47] Bosworth J K, Black C T and Ober C K 2009 Selective area control of self-assembled pattern architecture using a lithographically patternable block copolymer *ACS Nano* **3** 1761–6
[48] Paik M Y, Bosworth J K, Smilges D, Schwartz E L and Ober C K 2010 Reversible morphology control in block copolymer films via solvent vapor processing: an *in situ* GISAXS study *Macromolecules* **43** 4253–60
[49] Sun G *et al* Nanoscopic cylindrical dual concentric and lengthwise block brush terpolymers as covalent

preassembled high-resolution and high-sensitivity negative-tone photoresist materials *J. Am. Chem. Soc.* **135** 4203–6

[50] Maeda R, Hayakawa T and Ober C K 2012 Dual mode patterning of fluorine-containing block copolymers through combined top-down and bottom-up lithography *Chem. Mater.* **24** 1454–61

[51] Han E, Leolukman M, Kim M and Gopalan P 2010 Resist free patterning of nonpreferential buffer layers for block copolymer lithography *ACS Nano* **4** 6527–34

[52] Jung Y S, Jung W, Tuller H L and Ross C A 2008 Nanowire conductive polymer gas sensor patterned using self-assembled block copolymer lithography *Nano Lett.* **8** 3776–80

[53] Son J G, Son M, Moon K-J, Lee B H, Myoung J-M, Strano M S, Ham M-H and Ross C A 2013 Sub-10 nm graphene nanoribbon array field-effect transistors fabricated by block copolymer lithography *Adv. Mater.* **25** 4723–8

[54] Kathrein C C, Bai W, Currivan-Incorvia J A, Liontos G, Ntetsikas K, Avgeropoulos A, Böker A, Tsarkova L and Ross C A 2015 Combining graphoepitaxy and electric fields toward uniaxial alignment of solvent-annealed polystyrene–B–poly(dimethylsiloxane) block copolymers *Chem. Mater.* **27** 6890–8

[55] Chao C-C, Wang T-C, Ho R-M, Georgopanos P, Avgeropoulos A and Thomas E L 2010 Robust block copolymer mask for nanopatterning polymer films *ACS Nano* **4** 2088–94

[56] Li T, Wang Z, Schulte L and Ndoni S 2015 Substrate tolerant direct block copolymer nanolithography *Nanoscale* **8** 136–40

[57] Bellas V, Iatrou H and Hadjichristidis N 2000 Controlled anionic polymerization of hexamethylcyclotrisiloxane. Model linear and miktoarm star Co- and terpolymers of dimethylsiloxane with styrene and isoprene *Macromolecules* **33** 6993–7

[58] Politakos N, Ntoukas E, Avgeropoulos A, Krikorian V, Pate B D, Thomas E L and Hill R M 2009 Strongly segregated cubic microdomain morphology consistent with the double gyroid phase in high molecular weight diblock copolymers of polystyrene and poly(dimethylsiloxane) *J. Polym. Sci.* B **47** 2419–27

[59] O'Driscoll B M D, Kelly R A, Shaw M, Mokarian-Tabari P, Liontos G, Ntetsikas K, Avgeropoulos A, Petkov N and Morris M A 2013 Achieving structural control with thin polystyrene-B-polydimethylsiloxane block copolymer films: the complex relationship of interface chemistry, annealing methodology and process conditions *Eur. Polym. J.* **49** 3445–54

[60] Ma B, Zhou X, Wang G, Dai Z, Qin J and Lin B 2007 A hybrid microdevice with a thin PDMS membrance on the detection window for UV absorbance detection *Electrophoresis* **28** 2474–7

[61] Graubner V M, Jordan R, Nuyken O, Lippert T, Hauer M, Schnyder B and Wokaun A 2002 Incubation and ablation behavior of poly(dimethylsiloxane) for 266 nm irradiation *Appl. Surf. Sci.* **197–198** 786–90

[62] Bui V-T, Lee H S, Choi J-H and Choi H-S 2015 Data from crosslinked PS honeycomb thin film by deep UV irradiation *Data Br.* **5** 990–4

[63] Palacios M, García O and Rodríguez-Hernández J 2013 Constructing robust and functional micropatterns on polystyrene surfaces by using deep UV irradiation *Langmuir* **29** 2756–63

[64] Savas T A, Shah S N, Schattenburg M L, Carter J M and Smith H I 1995 Achromatic interferometric lithography for 100 nm-period gratings and grids *J. Vac. Sci. Technol.* B (*The 38th Int. Symp. electron, ion, Phot. beams*) **13** 2732–5

[65] NIST Chemistry Webbook (webbook.nist.gov/chemisty/)

[66] Kim J M, Kim Y, Park W I, Hur Y H, Jeong J W, Sim D M, Baek K M, Lee J H, Kim M-J and Jung Y S 2015 Eliminating the trade-off between the throughput and pattern quality of sub-15 nm directed self-assembly via warm solvent annealing *Adv. Funct. Mater.* **25** 306–15

[67] Park W I, Kim K, Jang H-I, Jeong J W, Kim J M, Choi J, Park J H and Jung Y S 2012 Directed self-assembly with sub-degrees Celsius processing temperature, sub-10 nanometer resolution, and sub-1 minute assembly time *Small* **8** 3762–8

[68] Hannon A F, Bai W, Alexander-Katz A and Ross C A 2015 Simulation methods for solvent vapor annealing of block copolymer thin films *Soft Matter* **11** 3794–9805

[69] Bai W, Yager K G and Ross C A 2016 *In situ* GISAXS study of a Si-containing block copolymer under solvent vapor annealing: effects of molecular weight and solvent vapor composition *Polymer* **101** 176–83

[70] Zhang Z, Fang S and Bao G 1999 Synthesis and characterization of polydimethylsiloxane/polystyrene semiinterpenetrating polymer networks *Chin. J. Polym. Sci.* **17** 537–42 (http://www.cjps.org/EN/Y1999/V17/I6/537)

[71] Rieger J 1996 The glass transition temperature of polystyrene *J. Therm. Anal.* **46** 965–72

[72] Koenhen D M and Smolders C A 1975 The determination of solubility parameters of solvents and polymers by means of correlations with other physical quantities *J. Appl. Polym. Sci.* **19** 1163–79

[73] Sakurai S 2008 Progress in control of microdomain orientation in block copolymers—efficiencies of various external fields *Polymer (Guildf)* **49** 2781–96